doi:10.2533/chimia.2023.132 Chimia 77 (2023) 132–138

Operando Photoelectron Photoion Coincidence Spectroscopy to Detect Short-lived Intermediates in Catalysis

Zihao Zhang[a], Javier Pérez-Ramírez[b], Jeroen A. van Bokhoven[bc], Andras Bodi*[a], and Patrick Hemberger*[a]

Abstract: Understanding the reaction mechanism is critical yet challenging in heterogeneous catalysis. Reactive intermediates, *e.g.*, radicals and ketenes, are short-lived and often evade detection. In this review, we summarize recent developments with *operando* photoelectron photoion coincidence (PEPICO) spectroscopy as a versatile tool capable of detecting elusive intermediates. PEPICO combines the advantages of mass spectrometry and the isomer-selectivity of threshold photoelectron spectroscopy. Recent applications of PEPICO in understanding catalyst synthesis and catalytic reaction mechanisms involving gaseous and surface-confined radical and ketene chemistry will be summarized.

Keywords: Catalysis · Elusive intermediates · Photoionization · Reaction mechanism · VUV

Zihao Zhang completed his PhD in chemical engineering at Zhejiang University in Sep 2019. From January 2018 to July 2019, he was a visiting PhD student at the University of Tennessee. From Oct 2019 to Oct 2021, he was a postdoctoral fellow at Pacific Northwest National Laboratory. Since Nov 2021, he has been working as a postdoctoral fellow at Paul Scherrer Institute. His research interests are the conversion of fossil and biomass feedstocks to fuels and chemicals.

Javier Pérez-Ramírez is Full Professor of Catalysis Engineering at ETH Zurich since 2010. His research pursues the nanoscale design of catalytic materials enabling the transition towards sustainable chemical and energy production. He directs NCCR Catalysis (www.nccr-catalysis.ch), a Swiss Centre of Competence in Research devoted to the development of carbon-neutral chemicals across the whole value chain through catalytic processes.

Jeroen A. van Bokhoven completed a degree in chemistry at Utrecht University (Netherlands) in 1995 and went on to obtain a PhD in inorganic chemistry and catalysis from the same university in 2000 (with honors). From 1999 until 2002 he was head of the XAS (X-ray absorption spectroscopy) users-support group at Utrecht University. In 2002, he moved to the ETH, where he worked as a Postdoc in the group of Professor Prins. In 2006 he obtained an SNF assistant professorship in the Department of Chemistry and Applied Biology. He was the 2008 recipient of the Swiss Chemical Society Werner Prize. Since 2010, Jeroen A. van Bokhoven has a Chair in Heterogeneous Catalysis at the Institute for Chemical and Bioengineering at ETH Zurich and is Head of Laboratory for Catalysis and Sustainable Chemistry at Paul Scherrer Institute.

Andras Bodi graduated from Eötvös University, Budapest, under the auspices of Prof. B. Sztáray and Prof. T. Baer (University of North Carolina). He joined the Paul Scherrer Institut in 2006 and constructed single and double imaging PEPICO endstations at the VUV beamline of the Swiss Light Source. Since 2006, PEPICO has grown from a fundamental physical chemistry technique through a unimolecular reaction microscope to a versatile analytical tool to unveil complex reaction mechanisms in catalysis. He has been leading the Reaction Dynamics Group since 2016.

Patrick Hemberger is a principal investigator and beamline scientist at the vacuum ultraviolet (VUV) beamline at PSI. He obtained his PhD degree in physical chemistry from the University of Würzburg (Germany) with Ingo Fischer in 2011. Patrick develops and applies photoelectron photoion coincidence (PEPICO) techniques utilizing VUV synchrotron radiation to unveil reaction mechanisms at all states, time scales, and phases. He received the Ružička Prize in Chemistry from ETH Zurich, was selected as a Mercator fellow by the German Science Foundation (DFG) and recently recognized for his significant contributions to the research field of energy in the Rising Stars special issue of *Energy and Fuels*.

1. Introduction

Active sites on the surface of a solid catalyst accelerate reaction rates selectively in heterogeneous catalysis.[1] Understanding

*Correspondence: Dr. A. Bodi[a], E-Mail: andras.boedi@psi.ch; Dr. P. Hemberger[a], E-Mail: patrick.hemberger@psi.ch

[a]Laboratory for Synchrotron Radiation and Femtochemistry, Paul Scherrer Institute, Villigen, Switzerland; [b]Institute of Chemical and Bioengineering, Department of Chemistry and Applied Biosciences, ETH Zurich, Zurich, Switzerland; [c]Laboratory for Catalysis and Sustainable Chemistry, Paul Scherrer Institute, CH-5232 Villigen, Switzerland

the catalytic reaction mechanism is challenging, because of the dynamic evolution of the active site during the reaction and the complex interplay between reactive intermediates, which determines the product distribution. Therefore, a two-pronged approach is most promising to unravel the reaction mechanism comprising a) monitoring of the active site under reaction conditions and b) revelation of reaction routes by detecting and identifying reactive intermediates liberated from the active site. The results from both are key to optimizing catalytic reactions to obtain high selectivities and conversion. To monitor the dynamic evolution of the active sites during the reaction, a series of *operando* characterization techniques have been developed, such as transmission electron microscopy (TEM),[2] infrared (IR) spectroscopy,[3] X-ray absorption spectroscopy (XAS),[4] near-ambient pressure X-ray photoelectron spectroscopy (XPS),[5] Raman,[6] X-ray diffraction (XRD),[7] and electron paramagnetic resonance (EPR) spectroscopy.[8]

In reactions yielding complex products, identifying the reaction intermediates, especially the weakly surface-bound ones liberated in the gas phase, is challenging yet fundamentally important to understand the catalysis mechanism. One of the major difficulties is that transient intermediates are usually present at low concentrations and their high reactivity and short lifetime allows them to evade detection by conventional sampling and detection techniques.[9] IR spectroscopy can distinguish the adsorbed reaction intermediates on the catalyst surface through fingerprints unique to functional groups.[10] However, the IR features of different species with similar molecular structure or functional groups often overlap, making the identification of intermediates difficult or impossible. This has led to a reliance on theoretical predictions in the study of reaction pathways and mechanisms.[11] Fortunately, in addition to IR spectroscopy, there are two emerging techniques to make the detection of short-lived intermediates possible.[12] The first one is (quasi) *operando* solid-state nuclear magnetic resonance (NMR) spectroscopy,[13] which enables the observation of chemical bonds and their interaction environment with the catalyst surface by analyzing various nuclear constituents (^{1}H, ^{13}C, ^{17}O, *etc*.). With 2-dimensional NMR, the chemical structure can often be inferred. Another, more direct approach is *operando* photoelectron photoion coincidence (PEPICO) spectroscopy,[14] which detects the intermediates desorbing from the catalyst surface directly and isomer-selectively by soft photoionization.

In this review, we will discuss recent advances in *operando* PEPICO spectroscopy at the VUV beamline of the Swiss Light Source and its applications in detecting elusive intermediates in the field of heterogeneous catalysis. We focus on four topics: (1) catalyst pretreatment such as redispersion of metal nanoparticles (NPs) into single-atom catalysts, (2) catalytic pyrolysis of lignin model compounds, (3) catalytic alkane activation, and (4) methanol- and methyl-chloride-to-hydrocarbon conversion (Scheme 1). The main elusive intermediates we detect are radicals and reactive oxygenates, such as ketenes. We will discuss their role during catalyst preparation and how they help reaction mechanism elucidation. Utilizing our expertise in reactive intermediates, novel sampling, and multiplex synchrotron detection techniques, we study reaction mechanisms as part of Work Page 3 (WP3, Advanced Tools) in NCCR Catalysis.

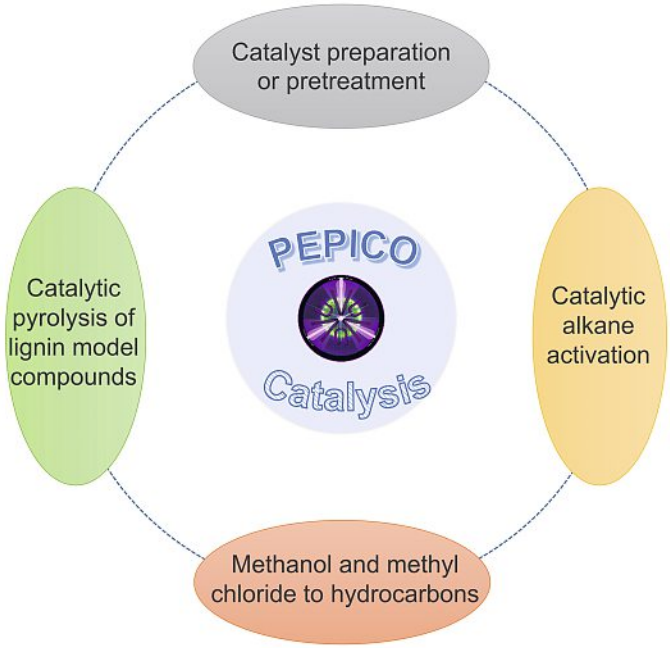

Scheme 1. Four recent application areas of PEPICO in the field of heterogeneous catalysis.

2. *Operando* PEPICO Spectroscopy

Time-of-flight mass spectrometry is a widely-used analytical approach for qualitative and quantitative analysis, commercialized in the early 1960s.[15] Among numerous ionization methods, electron ionization and photoionization are the most suitable to ionize small gaseous species universally. If more energy is transferred to the neutral molecule than its ionization energy upon interacting with the electron or the photon beam, a cation may be formed. In electron ionization, the large energy spread of thermally produced electrons and the broad energy transfer distribution means that dissociative ionization is difficult to suppress.[9b] In photoionization, the maximum of the internal energy transfer to the parent ion is the excess photon energy above the ionization energy (IE). However, if the photon energy is high, dissociative photoionization may readily yield fragments, which can be falsely assigned to a radical spectral carrier in a reactive mixture. For example, Li *et al.* recently reported the detection of methyl radicals ($CH_3^{\bullet}$) in methane activation,[16] based on the *m/z* 15 peak in the mass spectrum but without specifying the ionization energy. Given the comparable ethane signal in the same mass spectrum (IE(C_2H_6) = 11.52 eV vs. IE($CH_3^{\bullet}$) = 9.84 eV), the used photon energy must have exceeded 11.5 eV.[17] Therefore, the reader is left wondering if the *m/z* 15 peak could also be due to dissociative ionization rather than direct ionization of the methyl radical intermediate in methane activation. This shows why avoiding fragmentation or being able to distinguish dissociative photoionization from direct ionization is a prerequisite on the way to fully exploit photoionization mass spectrometry as an analytical tool.

Photoionization mass spectrometry (PIMS) with tunable vacuum ultraviolet (VUV) synchrotron light represents a sensitive, selective and multiplexed detection tool, corresponding to the first analytical dimension.[18] Although fragmentation can be suppressed in PIMS by choosing the photon energy judiciously, the distinction of isobars and isomers relies on differences in ionization energies and photoionization spectra.[19] These are often marginal, which often makes the isomer-selective assignment challenging, especially if more than two isomeric species or isomers with barely different ionization energies and photoionization spectra contribute to the signal. Photoelectrons are also emitted besides the photoion during photoionization. Bands in the photoelectron spectrum (PES) correspond to cation electronic states. The vibrational progression within a band follows the Franck–Condon principle and is often isomer-selective.[20] However, the photoelectron signal of the numerous products and the less intense signal of the intermediates are hopelessly intermingled when analyzing catalytic reactive environments with rich chemistry, which makes PES alone futile as an analytical tool. This limitation can be circumvented by coupling the photoelectron signal with photoion mass-selection, to record a photoelectron spectrum for each mass-to-charge chan-

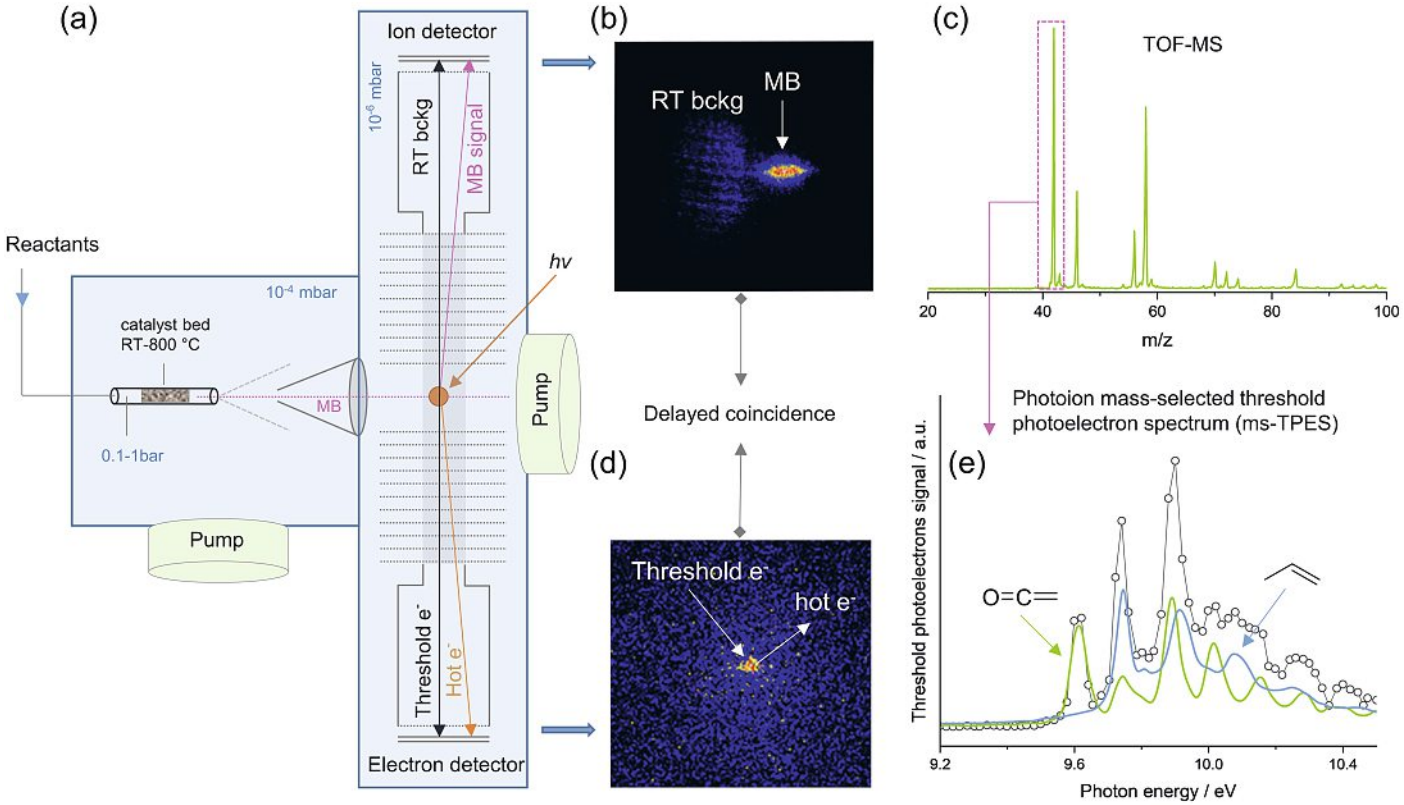

Fig. 1. (a) Scheme of *operando* PEPICO spectroscopy endstation; (b) photoion and (d) photoelectron VMI; (c) threshold photoionization mass spectrum (e) the photoion mass-selected threshold photoelectron spectrum of *m/z* 42.

nel. Precisely this is done in photoelectron photoion coincidence (PEPICO) spectroscopy,[21] when photoelectrons and -ions are detected in delayed coincidence to increase the selectivity of PIMS and allow for the study of complex mixtures.

The scheme of the *operando* PEPICO endstation can be found in Fig. 1a. Reactants are fed into the preheated reactor containing the catalyst bed. The inlet pressure of the reactor can be chosen from below 0.1 bar to ambient pressure depending on the reactor orifice, the amount of added catalyst, particle size, as well as the loading method. The reactor is placed in a vacuum chamber, and the effluent expands from the reactor into high vacuum (10^{-4} mbar) to form a molecular beam (MB). The MB travels through the skimmer to the second, ionization vacuum chamber (10^{-6} mbar). In the molecular beam, collisions are quickly suppressed and reactive intermediates (*e.g.,* radicals, ketenes, *etc*.) are frozen out and are not quenched after leaving the reactor. These species are softly photoionized with tunable and monochromatic VUV light to yield cations and photoelectrons. They are accelerated in opposite directions and detected in velocity map imaging (VMI) conditions in delayed coincidence by fast, position-sensitive delay-line detectors (Fig. 1b, d). Ions are also space focused on the detector, which, thanks to the almost instantaneous detection of the electron, allows us to record time-of-flight mass spectra (first analytical dimension).[9b] The VMI ion detector also measures the lateral momentum/velocity of each species, and the resulting 2-dimensional ion images (Fig. 1b) give rise to the second analytical dimension. Ion momentum analysis distinguishes direct ionization from fragmentation based on the kinetic energy release in the latter. It also discriminates the thermalized, scattered background signal in the ionization chamber (RT bckg in Fig. 1b), in which reactive species may be quenched, from the molecular beam signal (MB in Fig. 1b) due to direct ionization of the effluent from the reactor. Thanks to the tunability of the VUV photon energy and the high, in ideal cases *ca*. meV, resolution, dissociative ionization can be effectively suppressed. Together with the known photon energy, VMI photoelectron kinetic energy analysis delivers complete control over the photoionization energy balance and represents the third analytical dimension. By selecting only threshold photoelectrons within less than, *e.g*., 5 meV kinetic energy as start signal for the photoion TOF analysis, high-resolution photoion mass-selected threshold photoelectron spectra (ms-TPES) are obtained for each cation *m/z* channel. The *m/z* 42 ms-TPES is depicted in Fig. 1e,[22] which can be clearly assigned to a mixture of ketene ($H_2C{=}C{=}O$) and propylene. The assignment is based on reference spectra, available now for a myriad of reactive intermediates[20] and supported by Franck–Condon spectral modeling, which can reliably and routinely predict the vibrational structure of the ground-state band in the photoelectron spectrum nowadays.[23] PEPICO is a multiplexed technique and the ms-TPES is obtained for all *m/z* peaks in Fig. 1c simultaneously by scanning the photon energy and recording the threshold photoionization matrix.[24] Overall, this makes *operando* PEPICO spectroscopy a versatile tool to detect isomer-selectively elusive intermediates and stable products, present in the gas stream exiting the reactor either because they are weakly bound and desorbed from the catalyst or because they participate in gas-phase chemistry.[14a]

3. Applications of *Operando* PEPICO Spectroscopy

Universal, sensitive, (isomer-)selective, and multiplexed PEPICO detection has contributed to numerous topics in heterogeneous catalysis since 2017,[24] which we review in the following.

3.1 *Redispersion of Metal Nanoparticles into Single-atom Catalysts*

Sintering is one of the main causes of catalyst deactivation[25] and is driven by the decreased surface free energy at large particle size.[26] Redispersion of NPs into single-atoms is a strategy to maximize the utilization efficiency of metal atoms. For instance, Pt NPs will redisperse to single Pt-atoms (Pt_1) on the CeO_2 surface in the presence of O_2 at temperatures above 800 °C.[27] The mecha-

nism is hypothesized to involve the formation of volatile PtO_2 species from Pt NPs, followed by the migration and atom trapping by the CeO_2 surface. The redispersion of zeolite imidazolate framework-8 (ZIF-8) supported noble metal nanoparticles (Pt, Pd, and Au NPs) into single atoms occurs in an inert atmosphere above 900 °C.[28] Another low-temperature redispersion method of Ir and Pd NPs on activated carbon (AC) was realized in the presence of CO and CH_3I at about 325 °C.[29] X-ray absorption spectroscopy (XAS) was used to reveal the local coordination environment of the Ir_1 and Pd_1 catalysts, $Ir(CO)_2I_3$(O-AC) and $[Pd(CO)I_4(O\text{-}AC)]^{2-}$. However, the intermediates during the NPs redispersion process under thermal treatment in CO/CH_3I are difficult to capture by standard lab-based characterization techniques.

Since the detected intermediates for the redispersion of Pd and Ir NPs by PEPICO spectroscopy are similar,[29b,30] we focus on the latter. The redispersion is initiated by the homolytic cleavage of H_3C–I, which is observed already at low temperatures by the detection of I• (*m/z* 127) and CH_3• (*m/z* 15, Fig. 2a). By comparing the temperature-dependent I• (Fig. 2b) and CH_3•[29a] signals, the latter shows up only above 790 K, much higher than I• (605 K). This is mainly because of the formation of C_2H_6 (*m/z* 30) and C_2H_4 (*m/z* 28) at low temperatures, which consumes CH_3•. Other CH_3•-mediated products are also observed, such as CH_3OH (*m/z* 32) and CH_3COI (*m/z* 170, Fig. 2a). More importantly, the $Ir(CO)_3I$ complex (*m/z* 402 and 404) is also identified in the gas phase (Fig. 2a). It was found that Ir NPs cannot redisperse in N_2/CH_3I without CO,[29a] suggesting CO and CH_3I participate in the dispersive process of Ir NPs together by the formation of an $Ir(CO)_nI_m$ complex ($0 < n < m < 4$). The $Ir(CO)_nI_m$ complex binds AC surface oxygen to form Ir_1 (Fig. 2c). According to models of $Ir(CO)I_2$(O-AC), $Ir(CO)_2I$(O-AC), $Ir(CO)_3I$(O-AC), and $Ir(CO)_3I$, the last is most likely to escape from the surface, which explains why only $Ir(CO)_3I$ is found in the gas phase by PEPICO detection (Fig. 2c). Moreover, the detection of gaseous $Ir(CO)_3I$ also accounts for the slight metal leaching during the dispersion process. Overall, CO and I• will react with the metal atoms together at a gently elevated temperature to form volatile metal complexes. The formed Ir-containing complex is mobile, which can be trapped again on the surface by the surface oxygen on AC.

3.2 *Catalytic Pyrolysis of Lignin Model Compounds*

Lignocellulosic biomass is a cheap and abundant carbon-neutral feedstock for producing renewable value-added chemicals and biofuels.[31] Among the main conversion techniques, namely pyrolysis, gasification, and biochemical treatment, pyrolysis is the most economically feasible.[32] Bio-oil, the liquid product from biomass fast pyrolysis, has a low H/C ratio and high oxygen content compared to crude oil.[33] Bio-oil has to be upgraded by deoxygenation to be used as a replacement for gasoline and diesel.[34] An alternative is to upgrade the pyrolysis vapors prior to quenching to decrease the oxygen content over a solid catalyst in catalytic fast pyrolysis (CFP).[35] To understand the elementary reaction steps and the role and interaction of functional groups in the catalytic pyrolysis of biomass, the CFP of a series of lignin model compounds, among them methoxyphenol and benzenediol isomers, were studied using PEPICO detection. In 2017, the catalytic pyrolysis of guaiacol (**3**) in Fig. 3a over an H-USY zeolite catalyst was analyzed by both GC/MS and PEPICO[24] detection. Fulvenone (**15**) was found to be the key intermediate, produced by demethylation of guaiacol to catechol (**6**) and subsequent intramolecular dehydration. **15** is responsible for the formation of phenol (**7**) and cyclopentadiene (**12**). Cyclopentadiene (**12**) and fulvene (**14**) could only be detected by PEPICO spectroscopy because they do not survive in GC/MS sampling.

Free methyl radicals were also detected and were established to be derived from the methoxy group of guaiacol by ^{13}C labeling. The numerous methylation products, including methylcyclopentadienes (**13**), can therefore be rationalized based on the abundance of surface methyl species. In the CFP of the three benzenediol isomers (**4**,**5**,**6**) over H-ZSM-5, only catechol yields fulvenone ketene (**15**) by intramolecular dehydration (Fig. 3b).[36] Thus, fulvenone formation is driven by the proximity of the vicinal hydroxyl groups. The presence of this fulvenone-mediated reaction route also results in higher catechol catalytic reactivity compared to other two isomers. Analogously, the three methoxyphenol isomers (**1**,**2**,**3**) were also catalytically pyrolyzed, and the highest reactivity was found in the *ortho*-substituted guaiacol (**3**).[37] Additionally, PEPICO identified the naphthalene (**17**)

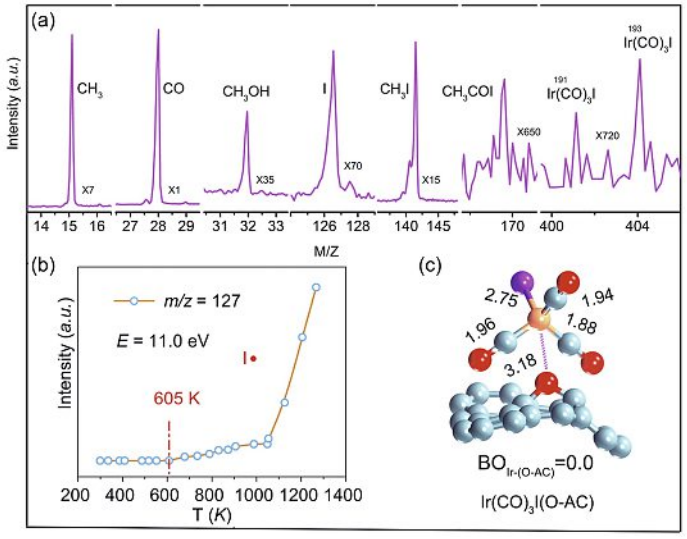

Fig. 2. (a) Photoionization mass spectrum, (b) temperature dependence of the I• signal during dispersal of Ir NPs with CO/CH_3I; (c) model of $Ir(CO)_3I$(O-AC). Reproduced from ref. [29a,30] with permission. Copyright 2020 Elsevier Inc.

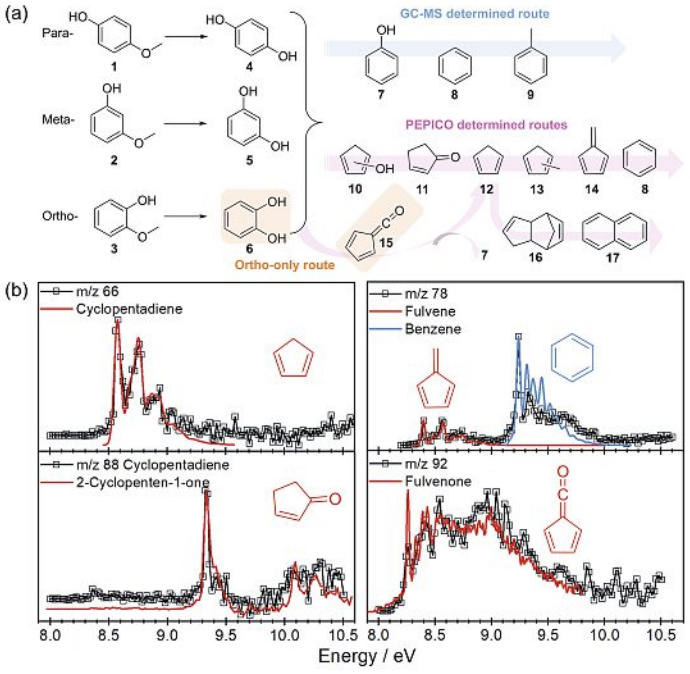

Fig. 3. (a) Reaction routes in the CFP of lignin model compounds, determined by GC/MS and PEPICO; (b) ms-TPES of representative intermediates in catechol CFP. Figure 3(b) is reproduced from ref. [36] with permission from the Royal Society of Chemistry.

formation route by cyclopentadiene (**12**) dimerization yielding dicyclopentadiene (**16**) as one of the key early intermediates in coke formation.

Overall, while GC/MS only detects stable species, PEPICO spectroscopy identified fleeting catalysis intermediates and the fulvenone route in the catalytic pyrolysis of lignin model compounds. By studying the conversion of stable intermediates as reactants, such as 2-cyclopeten-1-one (**11**), phenol (**7**), cyclopentadiene (**12**), *etc.*,[36] the catalytic mechanism could be refined, furthering our understanding of the CFP process. More specifically, the fulvenone-mediated reaction route was found to be limited to the *ortho*-isomers **3** and **6**, and is the driving force of their higher catalytic pyrolysis activity.

3.3 *Alkane Functionalization*

In addition to the use of natural gas as a non-renewable energy source,[38] the selective production of olefins, alcohols, aromatics *etc*. from alkanes, the major constituent of natural gas, is alluring in the transition from the fossil to the renewables era.[39] However, in the absence of feasible valorization approaches for inert C_{1-4} alkanes, large amounts of gaseous oil extraction by-products are flared. Catalytic alkane activation can in fact be realized at moderate temperatures.[40] In methane oxybromination over $(VO)_2P_2O_7$ and EuOBr catalysts, bromine radicals were observed already at lower temperatures than methyl radicals.[41] Combined with density functional theory calculations and kinetics data, a gas-phase CH_4 activation route was identified, which proceeds by surface oxidation of HBr to Br$^\bullet$, which desorbs and activates CH_4 in the gas phase to $CH_3^\bullet$ directly (Fig. 4a). The analogous reaction pathway was also verified in methane oxybromination over Pd/SiO_2.[42] However, chlorine radicals (Cl$^\bullet$) can only be found in small concentration with HCl and O_2 as reactants, and the signal disappears in oxychlorination when CH_4 is co-fed. The absence of Cl$^\bullet$ is due to rapid CH_4 activation. Furthermore, based on the halogen evolution rate in HX oxidation and methane oxyhalogenation, gas-phase chemistry is dominant in CH_4 oxybromination and marginal in oxychlorination.

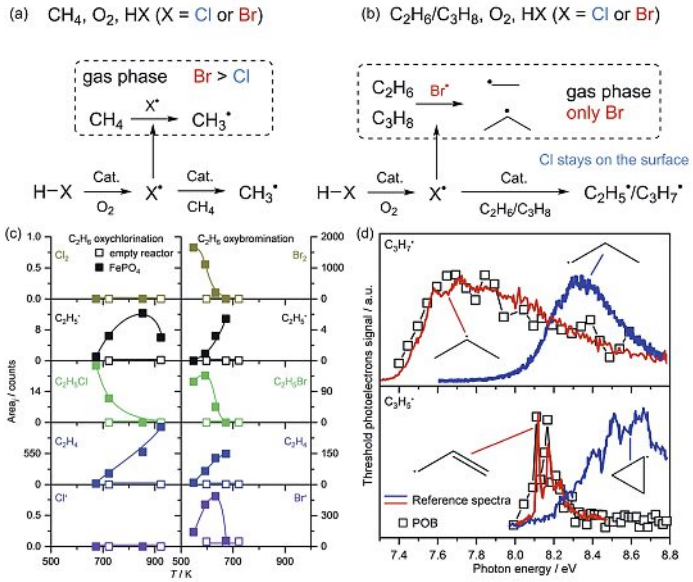

Fig. 4. Surface and gas-phase alkane activation mechanism in (a) methane oxyhalogenation, (b) ethane and propane oxyhalogenation over different catalysts; (c) Peak areas of various species as a function of temperature in ethane oxychlorination and oxybromination; (d) ms-TPES of $C_3H_7^\bullet$ and $C_3H_5^\bullet$ in propane oxybromination. (c) is adapted with permission from ref. [43]. Copyright John Wiley & Sons, Inc. (d) is reprinted with permission from ref. [45]. Copyright 2020 American Chemical Society.

Ethane oxybromination and oxychlorination were also compared over $FePO_4$.[43] Similarly to the methane results, the large Br$^\bullet$ and Br_2 signals were in contrast to the absence of the Cl$^\bullet$ and Cl_2 peaks (Fig. 4c). Prompt-gamma activation analysis (PGAA), a surface-coverage quantification technique,[44] indicated high surface Cl density (4.1 $mmol_{Cl}mol_{Fe}^{-1}$) at 723 K, which decreased to 3 $mmol_{Cl}mol_{Fe}^{-1}$ at 773 K. The surface Br density was 2.5 $mmol_{Br}mol_{Fe}^{-1}$ at 663 K, and Br vanished from the surface at 723 K. Thus, Br$^\bullet$ escapes the surface and participates in the gas-phase reaction route, while ethane oxychlorination only contains surface-confined functionalization (Fig. 4b). Isomer-selective analysis of intermediates unveiled mechanistic insights into propane oxyhalogenation over $CrPO_4$. Again, Br$^\bullet$ and Br_2[45] were found in oxybromination, while Cl$^\bullet$ and Cl_2 were absent in surface-confined oxychlorination (Fig. 4b). Gas-phase C–H activation products in oxybromination of propane and propene were isomer-selectively assigned as isopropyl (*i*-$C_3H_7^\bullet$, thermodynamically more stable than *n*-$C_3H_7^\bullet$) and allyl radicals ($C_3H_5^\bullet$), respectively, based on the ms-TPES (Fig. 4d). The propargyl radical ($C_3H_3^\bullet$) was also detected and is likely produced by consecutive H abstraction. It is one of the key benzene formation intermediates and largely responsible for early coke formation.

Propargyl was also identified in non-oxidative methane coupling over $Fe@SiO_2$[46] and was recognized as rapid C_6 formation intermediate, besides the stepwise C_1 addition reaction. Here, $CH_3^\bullet$ radicals were formed over both fresh $Fe@SiO_2$ and SiO_2 catalysts, but C_{2+} radicals were only observed over $Fe@SiO_2$ in the early stages of the reaction. This suggests that the initial $CH_3^\bullet$ coupling takes place on the iron site. However, pre-coked $Fe@SiO_2$ and SiO_2 showed similar C_{2+} radical and C_{2+} product distribution, which indicates that the active sites of $Fe@SiO_2$ and SiO_2 change during the reaction. Be it in oxidative or non-oxidative environments, detecting reactive intermediates with *operando* techniques provides deep mechanistic insights, which help make these processes more economically viable.

3.4 *Methanol and Methyl Chloride to Hydrocarbons*

Production of high-demand chemical commodities such as hydrocarbons from monosubstituted methyl chloride and methanol, CH_3X (X = halogen, OH), has also attracted much attention in academia and industry.[47] Methyl halide-to-hydrocarbons (*e.g.*, MCTH for CH_3Cl) and methanol-to-hydrocarbon reactions (MTH) were widely studied over zeolite catalysts, particularly ZSM-5 and SAPO-34.[48] The main products from these reactions are C_2–C_5 alkenes, alkanes, and aromatics. SAPO-34 produces more light alkenes compared to ZSM-5 due to the narrow cavity openings.[48] The reaction mechanism, especially in the induction period, is still hotly debated.[11a,14b,49] By monitoring MCTH and MTH with *operando* PEPICO at low and near-ambient pressures, we observed $CH_3^\bullet$ radicals in both reactions and ketene only in MTH.[14b] After analyzing the temperature-dependent evolution of the reaction intermediates, C–C bond formation and propagation routes were proposed (Fig. 5a,b). $CH_3^\bullet$-addition routes dominate in MCTH, *i.e.,* C_2H_4 formation by C–C coupling and hydrogen transfer, followed by further methylation to form C_3–C_5 hydrocarbons (Fig. 5b). In MTH, an oxygenate-driven route was found besides the $CH_3^\bullet$-addition route (Fig. 5a). First, HCHO derived from CH_3OH or $(CH_3)_2O$ dehydrogenates to CO. Second, Koch-carbonylation of oxygenates generates the first C–C bond product, ketene. Finally, olefins are formed from ketene *via* decarbonylation. It should be noted that ketene is considered as the key intermediate to olefin formation, as also reported for the syngas-to-olefins process.[13d,50] Despite ketene being observed in MTH for the first time by PEPICO[14b] spectroscopy, its role in the initiation phase of the reaction could only be investigated theoretically until now, owing to its low stability and concentration.

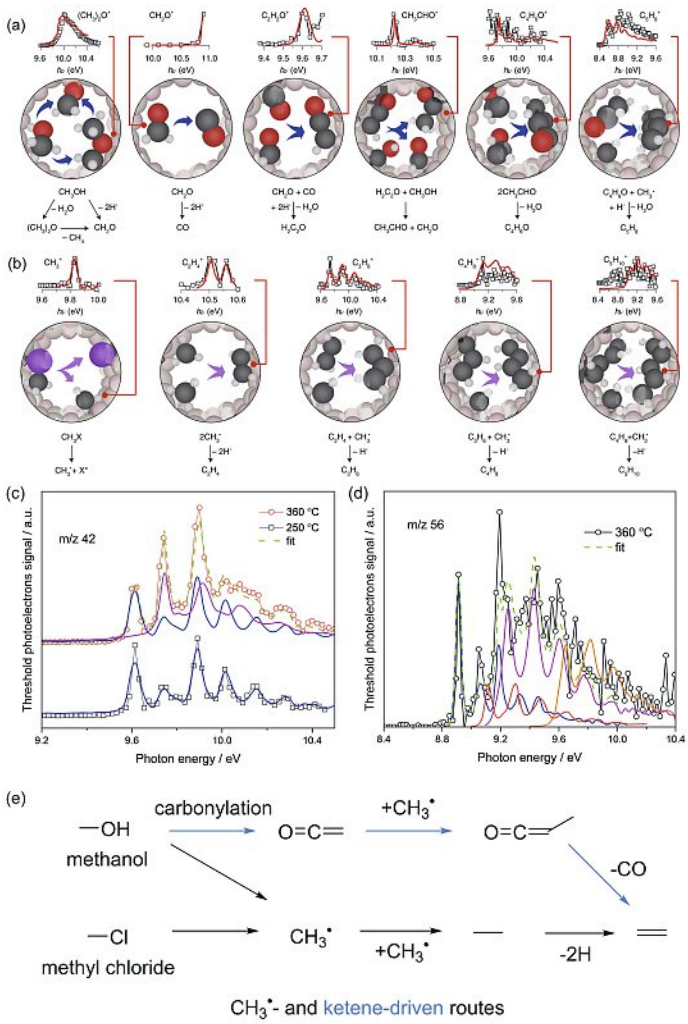

Fig. 5. (a,b) Proposed reaction network of the oxygenate-driven reaction in MTH and $CH_3^•$ radical-addition pathway in both MTH and MCTH over HZSM-5; (c,d) typical *m/z* 42 and 56 ms-TPES in methyl acetate conversion over HZSM-5; (e) C_2H_4 formation routes from $CH_3^•$ radical-addition and ketene-driven routes. Figs 5(a,b) are reprinted from ref. [14b]. Figs 5(c,d) are reprinted from ref. [22].

To unveil the role of ketenes during the initiation phase of the MTH reaction, methyl acetate was selected as precursor to produce ketene over an HZSM-5 catalyst at a low reaction temperature of 250 °C.[22] No olefins were formed at these low temperatures (Fig. 5c), however by increasing the reaction temperature to 360 °C, a secondary intermediate, methylketene, could be detected (Fig. 5d), while C_{2-5} olefins were produced simultaneously. The formation of methylketene clearly indicates ethenone ketene methylation at higher temperatures. Due to the abundance of Brønsted acid sites on HZSM-5, a rapid equilibrium sets in between ethenone ketene and surface acetyl[50b] and, analogously, methylketene and surface propionyl. Decarbonylation of methylketene, or of the corresponding surface propionyl, yields the first olefin, C_2H_4, proving the proposed ketene-driven route[11] experimentally for the first time. C_2H_4 formation routes by $CH_3^•$ radical addition and ketene-driven routes in MTH and MCTH, revealed by PEPICO detection, are summarized in Fig. 5e.

4. Conclusions

PEPICO detects short-lived intermediates, such as radicals and ketenes, isomer-selectively. These elusive species define reaction mechanisms, the understanding of which can contribute to rational catalyst and process design. In this review, we highlight how PEPICO has answered mechanistic questions about (1) catalyst preparation, (2) elementary reactions in biomass valorization, (3) alkane functionalization, and (4) methanol- as well as methylchloride-to-hydrocarbon processes. The gas-phase chemistry during the redispersion of single-atom catalysts reveals the dispersion chemistry and the origin of metal leaching. The abundance of free radicals, oxygenates, and other intermediates in the gas phase as well as their ratio does not only reveal the elementary steps but also gives a clue to the role of gaseous and surface-contained chemistry.

PEPICO only detects intermediates that desorb from the catalyst surface, although desorption can be facilitated at low pressures. However, strongly bound surface intermediates remain challenging to detect. Surface-sensitive techniques (*i.e.*, EPR, IR, NMR, PGAA, *etc*.) can, thus, provide complementary results to complete the mechanism.[13b,14b] Co-feeding an internal standard (*e.g*., Xe) allows us to obtain mole fractions of reaction intermediates and products,[14b] but absolute yields remain elusive in the absence of species and photon energy dependent photoionization cross sections (PICS). Although the PICS of two crucial ketene intermediates could be quantified in salicylamide pyrolysis, fulvenone, and 2-carbonyl cyclohexadienone,[51] such dearly needed measurements of fleeting intermediates remain the Holy Grail of photoionization studies for reliable quantification.

Acknowledgements

This publication was created as part of NCCR Catalysis (grant number 180544), a National Centre of Competence in Research funded by the Swiss National Science Foundation. The experiments were performed at the VUV beamline of the Swiss Light Source located at Paul Scherrer Institute. P.H. acknowledges funding by the SNSF under grant number 200021_178952.

Received: December 6, 2022

[1] R. Schlögl, *Angew. Chem. Int. Ed.* **2015**, *54*, 3465, https://doi.org/10.1002/anie.201410738.

[2] a) W. Yuan, B. Zhu, K. Fang, X.-Y. Li, T. W. Hansen, Y. Ou, H. Yang, J. B. Wagner, Y. Gao, Y. Wang, *Science* **2021**, *371*, 517, https://doi.org/10.1126/science.abe3558; b) H. Frey, A. Beck, X. Huang, J. A. van Bokhoven, M.-G. Willinger, *Science* **2022**, *376*, 982, https://doi.org/10.1126/science.abm3371.

[3] a) I. X. Green, W. Tang, M. Neurock, J. T. Yates Jr, *Science* **2011**, *333*, 736, https://doi.org/10.1126/science.1207272; b) K. Ding, A. Gulec, A. M. Johnson, N. M. Schweitzer, G. D. Stucky, L. D. Marks, P. C. Stair, *Science* **2015**, *350*, 189, https://doi.org/10.1126/science.aac6368; c) J. Ryczkowski, *Catal. Today* **2001**, *68*, 263, https://doi.org/10.1016/S0920-5861(01)00334-0.

[4] a) F. Maurer, J. Jelic, J. Wang, A. Gänzler, P. Dolcet, C. Wöll, Y. Wang, F. Studt, M. Casapu, J.-D. Grunwaldt, *Nat. Catal.* **2020**, *3*, 824, https://doi.org/10.1038/s41929-020-00508-7; b) C. H. van Oversteeg, H. Q. Doan, F. M. de Groot, T. Cuk, *Chem. Soc. Rev.* **2017**, *46*, 102, https://doi.org/10.1039/C6CS00230G; c) A. Marberger, A. W. Petrov, P. Steiger, M. Elsener, O. Kröcher, M. Nachtegaal, D. Ferri, *Nat. Catal.* **2018**, *1*, 221, https://doi.org/10.1038/s41929-018-0032-6.

[5] a) Z. Liu, E. Huang, I. Orozco, W. Liao, R. M. Palomino, N. Rui, T. Duchoň, S. Nemšák, D. C. Grinter, M. Mahapatra, *Science* **2020**, *368*, 513, https://doi.org/10.1126/science.aba5005; b) V. Muravev, G. Spezzati, Y.-Q. Su, A. Parastaev, F.-K. Chiang, A. Longo, C. Escudero, N. Kosinov, E. J. Hensen, *Nat. Catal.* **2021**, *4*, 469, https://doi.org/10.1038/s41929-021-00621-1.

[6] Q. Wang, Y. Li, A. Serrano-Lotina, W. Han, R. Portela, R. Wang, M. A. Bañares, K. L. Yeung, *J Am. Chem. Soc.* **2020**, *143*, 196, https://doi.org/10.1021/jacs.0c08640.

[7] F. Zhang, Z. Liu, X. Chen, N. Rui, L. E. Betancourt, L. Lin, W. Xu, C. Sun, A. M. Abeykoon, J. A. Rodriguez, *ACS Catal.* **2020**, *10*, 3274, https://doi.org/10.1021/acscatal.9b04451.

[8] a) Y. Wu, Y. Ma, Y. Wang, K. G. Rappé, N. M. Washton, Y. Wang, E. D. Walter, F. Gao, *J Am. Chem. Soc.* **2022**, *144*, 9734, https://doi.org/10.1021/jacs.2c01933; b) G. Zichittella, Y. Polyhach, R. Tschaggelar, G. Jeschke, J. Pérez-Ramírez, *Angew. Chem.* **2021**, *133*, 3640, https://doi.org/10.1002/ange.202013331.

[9] a) P. Hemberger, A. Bodi, T. Bierkandt, M. Köhler, D. Kaczmarek, T. Kasper, *Energy Fuels* **2021**, *35*, 16265, https://doi.org/10.1021/acs.energyfuels.1c01712; b) P. Hemberger, J. A. van Bokhoven, J. Pérez-Ramírez, A. Bodi, *Catal. Sci. Technol.* **2020**, *10*, 1975, https://doi.org/10.1039/C9CY02587A.

[10] N. J. Firet, W. A. Smith, *ACS Catal.* **2017**, *7*, 606, https://doi.org/10.1021/acscatal.6b02382.
[11] a) P. N. Plessow, A. Smith, S. Tischer, F. Studt, *J Am. Chem. Soc.* **2019**, *141*, 5908, https://doi.org/10.1021/jacs.9b00585; b) P. N. Plessow, F. Studt, *ACS Catal.* **2017**, *7*, 7987, https://doi.org/10.1021/acscatal.7b03114.
[12] S.-M. Wu, M. Beller, X.-Y. Yang, *Matter* **2022**, *5*, 3104, https://doi.org/10.1016/j.matt.2022.09.006.
[13] a) X. Tang, W. Chen, X. Yi, Z. Liu, Y. Xiao, Z. Chen, A. Zheng, *Angew. Chem.* **2021**, *133*, 4631, https://doi.org/10.1002/ange.202013384; b) Y. Ji, P. Gao, Z. Zhao, D. Xiao, Q. Han, H. Chen, K. Gong, K. Chen, X. Han, X. Bao, *Nat. Catal.* **2022**, *5*, 594, https://doi.org/10.1038/s41929-022-00806-2; c) N. R. Jaegers, K. T. Mueller, Y. Wang, J. Z. Hu, *Acc. Chem. Res.* **2020**, *53*, 611, https://doi.org/10.1021/acs.accounts.9b00557; d) Y. Zhang, P. Gao, F. Jiao, Y. Chen, Y. Ding, G. Hou, X. Pan, X. Bao, *J Am. Chem. Soc.* **2022**, *144*, 18251, https://doi.org/10.1021/jacs.2c03478.
[14] a) A. Bodi, P. Hemberger, J. Pérez-Ramírez, *Nat. Catal.* **2022**, *5*, 850, https://doi.org/10.1038/s41929-022-00847-7; b) A. Cesarini, S. Mitchell, G. Zichittella, M. Agrachev, S. P. Schmid, G. Jeschke, Z. Pan, A. Bodi, P. Hemberger, J. Pérez-Ramírez, *Nat. Catal.* **2022**, *5*, 605, https://doi.org/10.1038/s41929-022-00808-0.
[15] N. Mirsaleh-Kohan, W. D. Robertson, R. N. Compton, *Mass Spectrom. Rev.* **2008**, *27*, 237, https://doi.org/10.1002/mas.20162.
[16] Z. Li, Y. Xiao, P. R. Chowdhury, Z. Wu, T. Ma, J. Z. Chen, G. Wan, T.-H. Kim, D. Jing, P. He, *Nat. Catal.* **2021**, *4*, 882, https://doi.org/10.1038/s41929-021-00686-y.
[17] https://www.nist.gov/
[18] a) D. L. Osborn, P. Zou, H. Johnsen, C. C. Hayden, C. A. Taatjes, V. D. Knyazev, S. W. North, D. S. Peterka, M. Ahmed, S. R. Leone, *Rev. Sci. Instrum.* **2008**, *79*, 104103, https://doi.org/10.1063/1.3000004; b) L. Luo, R. You, Y. Liu, J. Yang, Y. Zhu, W. Wen, Y. Pan, F. Qi, W. Huang, *ACS Catal.* **2019**, *9*, 2514, https://doi.org/10.1021/acscatal.8b04728; c) Y. Yang, X. Guo, Y. Pan, Y. Fang, *Catal. Sci. Technol.* **2022**, *12*, 1746, https://doi.org/10.1039/D1CY02102H.
[19] B. Sztáray, K. Voronova, K. G. Torma, K. J. Covert, A. Bodi, P. Hemberger, T. Gerber, D. L. Osborn, *J. Chem. Phys.* **2017**, *147*, 013944, https://doi.org/10.1063/1.4984304.
[20] J. M. Dyke, *Phys. Chem. Chem. Phys.* **2019**, *21*, 9106, https://doi.org/10.1039/C9CP00623K.
[21] T. Baer, R. P. Tuckett, *Phys. Chem. Chem. Phys.* **2017**, *19*, 9698, https://doi.org/10.1039/C7CP00144D.
[22] X. Wu, Z. Zhang, Z. Pan, X. Zhou, A. Bodi, P. Hemberger, *Angew. Chem. Int. Ed.* **2022**, *134*, e202207777, https://doi.org/10.1002/ange.202207777.
[23] I. S. Ulusoy, J. A. Gomez, O. Vendrell, *J. Phys. Chem. A* **2019**, *123*, 8832, https://doi.org/10.1021/acs.jpca.9b07404.
[24] P. Hemberger, V. B. Custodis, A. Bodi, T. Gerber, J. A. van Bokhoven, *Nat. Commun.* **2017**, *8*, 15946, https://doi.org/10.1038/ncomms15946.
[25] A. J. Martin, S. Mitchell, C. Mondelli, S. Jaydev, J. Perez-Ramirez, *Nat. Catal.* **2022**, *5*, 854, https://doi.org/10.1038/s41929-022-00842-y.
[26] J. Lu, B. Fu, M. C. Kung, G. Xiao, J. W. Elam, H. H. Kung, P. C. Stair, *Science* **2012**, *335*, 1205, https://doi.org/10.1126/science.1212906.
[27] a) J. Jones, H. Xiong, A. T. DeLaRiva, E. J. Peterson, H. Pham, S. R. Challa, G. Qi, S. Oh, M. H. Wiebenga, X. I. Pereira Hernández, *Science* **2016**, *353*, 150, https://doi.org/10.1126/science.aaf8800; b) L. Nie, D. Mei, H. Xiong, B. Peng, Z. Ren, X. I. P. Hernandez, A. DeLaRiva, M. Wang, M. H. Engelhard, L. Kovarik, *Science* **2017**, *358*, 1419, https://doi.org/10.1126/science.aao2109; c) Y. Lu, Z. Zhang, F. Lin, H. Wang, Y. Wang, *ChemNanoMat* **2020**, *6*, 1659, https://doi.org/10.1002/cnma.202000407.
[28] S. Wei, A. Li, J.C. Liu, Z. Li, W. Chen, Y. Gong, Q. Zhang, W.C. Cheong, Y. Wang, L. Zheng, *Nat. Nanotechnol.* **2018**, *13*, 856, https://doi.org/10.1038/s41565-018-0197-9.
[29] a) S. Feng, P. Hemberger, A. Bodi, X. Song, T. Yu, Z. Jiang, Y. Liu, Y. Ding, *J. Catal.* **2020**, *382*, 347, https://doi.org/10.1016/j.jcat.2019.12.040; b) X. Li, S. Feng, P. Hemberger, A. Bodi, X. Song, Q. Yuan, J. Mu, B. Li, Z. Jiang, Y. Ding, *ACS Catal.* **2021**, *11*, 9242, https://doi.org/10.1021/acscatal.1c01579.
[30] S. Feng, X. Lin, X. Song, Y. Liu, Z. Jiang, P. Hemberger, A. Bodi, Y. Ding, *J. Catal.* **2020**, *381*, 193, https://doi.org/10.1016/j.jcat.2019.10.032.
[31] a) C. Liu, H. Wang, A. M. Karim, J. Sun, Y. Wang, *Chem. Soc. Rev.* **2014**, *43*, 7594, https://doi.org/10.1039/C3CS60414D; b) T. R. Carlson, G. A. Tompsett, W. C. Conner, G. W. Huber, *Top. Catal.* **2009**, *52*, 241, https://doi.org/10.1007/s11244-008-9160-6.
[32] R. P. Anex, A. Aden, F. K. Kazi, J. Fortman, R. M. Swanson, M. M. Wright, J. A. Satrio, R. C. Brown, D. E. Daugaard, A. Platon, *Fuel* **2010**, *89*, S29, https://doi.org/10.1016/j.fuel.2010.07.015.
[33] T. Dickerson, J. Soria, *Energies* **2013**, *6*, 514, https://doi.org/10.3390/en6010514.
[34] L. Qu, X. Jiang, Z. Zhang, X. Zhang, G. Song, H. Wang, Y. Yuan, Y. Chang, *Green Chem.* **2021**, *23*, 9348, https://doi.org/10.1039/D1GC03183J.
[35] R. Venderbosch, *ChemSusChem* **2015**, *8*, 1306, https://doi.org/10.1002/cssc.201500115.
[36] Z. Pan, A. Puente-Urbina, A. Bodi, J. A. van Bokhoven, P. Hemberger, *Chem. Sci.* **2021**, *12*, 3161, https://doi.org/10.1039/D1SC00654A.
[37] Z. Pan, A. Bodi, J. A. van Bokhoven, P. Hemberger, *Phys. Chem. Chem. Phys.* **2022**, *24*, 21786, https://doi.org/10.1039/D2CP02741K.
[38] L. Wei, P. Geng, *Fuel Process. Technol.* **2016**, *142*, 264, https://doi.org/10.1016/j.fuproc.2015.09.018.
[39] a)H. Chen, S. Schlecht, T. C. Semple, J. F. Hartwig, *Science* **2000**, *287*, 1995, https://doi.org/10.1126/science.287.5460.1995; b) J. Sheng, B. Yan, W.-D. Lu, B. Qiu, X.-Q. Gao, D. Wang, A.-H. Lu, *Chem. Soc. Rev.* **2021**, *50*, 1438, https://doi.org/10.1039/D0CS01174F; c) J. Grant, C. A. Carrero, F. Goeltl, J. Venegas, P. Mueller, S. P. Burt, S. Specht, W. McDermott, A. Chieregato, I. Hermans, *Science* **2016**, *354*, 1570, https://doi.org/10.1126/science.aaf7885; d) L. Li, X. Mu, W. Liu, X. Kong, S. Fan, Z. Mi, C. J. Li, *Angew. Chem.* **2014**, *126*, 14330, https://doi.org/10.1002/ange.201408754; e) M. Ravi, M. Ranocchiari, J. A. van Bokhoven, *Angew. Chem. Int. Ed.* **2017**, *56*, 16464, https://doi.org/10.1002/anie.201702550; f) V. Paunović, G. Zichittella, M. Moser, A. P. Amrute, J. Pérez-Ramírez, *Nature Chem.* **2016**, *8*, 803, https://doi.org/10.1038/nchem.2522.
[40] P. Tang, Q. Zhu, Z. Wu, D. Ma, *Energy Environ. Sci.* **2014**, *7*, 2580, https://doi.org/10.1039/C4EE00604F.
[41] V. Paunović, P. Hemberger, A. Bodi, N. López, J. Pérez-Ramírez, *Nat. Catal.* **2018**, *1*, 363, https://doi.org/10.1038/s41929-018-0071-z.
[42] V. Paunović, G. Zichittella, P. Hemberger, A. Bodi, J. Pérez-Ramírez, *ACS Catal.* **2019**, *9*, 1710, https://doi.org/10.1021/acscatal.8b04375.
[43] G. Zichittella, M. Scharfe, B. Puértolas, V. Paunović, P. Hemberger, A. Bodi, L. Szentmiklósi, N. López, J. Pérez-Ramírez, *Angew. Chem. Int. Ed.* **2019**, *58*, 5877, https://doi.org/10.1002/anie.201811669.
[44] Z. Révay, T. s. Belgya, L. s. Szentmiklósi, Z. n. Kis, A. Wootsch, D. Teschner, M. Swoboda, R. Schlögl, J. n. Borsodi, R. Zepernick, *Anal. Chem.* **2008**, *80*, 6066, https://doi.org/10.1021/ac800882k.
[45] G. Zichittella, P. Hemberger, F. Holzmeier, A. Bodi, J. Pérez-Ramírez, *J. Phys. Chem. Lett.* **2020**, *11*, 856, https://doi.org/10.1021/acs.jpclett.9b03836.
[46] A. Puente-Urbina, Z. Pan, V. Paunović, P. Šot, P. Hemberger, J. A. van Bokhoven, *Angew. Chem.* **2021**, *133*, 24204, https://doi.org/10.1002/ange.202107553.
[47] a) I. Yarulina, A. D. Chowdhury, F. Meirer, B. M. Weckhuysen, J. Gascon, *Nat. Catal.* **2018**, *1*, 398, https://doi.org/10.1038/s41929-018-0078-5; b) U. Olsbye, S. Svelle, M. Bjørgen, P. Beato, T. V. Janssens, F. Joensen, S. Bordiga, K. P. Lillerud, *Angew. Chem. Int. Ed.* **2012**, *51*, 5810, https://doi.org/10.1002/anie.201103657; c) D. Zhu, Z. Wang, F. Meng, B. Zhao, S. Kanitkar, Y. Tang, *Catal. Lett.* **2021**, *151*, 1038, https://doi.org/10.1007/s10562-020-03364-z.
[48] U. Olsbye, O. V. Saure, N. B. Muddada, S. Bordiga, C. Lamberti, M. H. Nilsen, K. P. Lillerud, S. Svelle, *Catal. Today* **2011**, *171*, 211, https://doi.org/10.1016/j.cattod.2011.04.020.
[49] a) Y. Liu, S. Müller, D. Berger, J. Jelic, K. Reuter, M. Tonigold, M. Sanchez-Sanchez, J. A. Lercher, *Angew. Chem.* **2016**, *128*, 5817, https://doi.org/10.1002/ange.201511678; b) K. Hemelsoet, J. Van der Mynsbrugge, K. De Wispelaere, M. Waroquier, V. Van Speybroeck, *ChemPhysChem* **2013**, *14*, 1526, https://doi.org/10.1002/cphc.201201023.
[50] a) F. Jiao, J. Li, X. Pan, J. Xiao, H. Li, H. Ma, M. Wei, Y. Pan, Z. Zhou, M. Li, *Science* **2016**, *351*, 1065, https://doi.org/10.1126/science.aaf1835; b) C.-M. Wang, Y.-D. Wang, Z.-K. Xie, *Catal. Sci. Technol.* **2016**, *6*, 6644, https://doi.org/10.1039/C6CY01095D; c) F. Jiao, X. Pan, K. Gong, Y. Chen, G. Li, X. Bao, *Angew. Chem. Int. Ed.* **2018**, *57*, 4692, https://doi.org/10.1002/anie.201801397.
[51] Z. Pan, A. Bodi, J. A. van Bokhoven, P. Hemberger, *Phys. Chem. Chem. Phys.* **2022**, *24*, 3655, https://doi.org/10.1039/D1CP05206C.